New Journal of Physics
The open-access journal for physics

Assessing one-dimensional diffusion in nanoporous materials from transient concentration profiles

Lars Heinke[1] **and Jörg Kärger**

Faculty of Physics and Geosciences, University of Leipzig, Linnéstrasse 5, 04103 Leipzig, Germany
E-mail: heinke@physik.uni-leipzig.de and kaerger@physik.uni-leipzig.de

New Journal of Physics **10** (2008) 023035 (25pp)
Received 19 December 2008
Published 22 February 2008
Online at http://www.njp.org/
doi:10.1088/1367-2630/10/2/023035

Abstract. The use of interference microscopy has enabled the direct observation of transient concentration profiles generated by intracrystalline transport diffusion in nanoporous materials. The thus accessible intracrystalline concentration profiles contain a wealth of information which cannot be deduced by any macroscopic method. In this paper, we illustrate five different ways for determining the concentration-dependent diffusivity in one-dimensional systems and two for the surface permeability. These methods are discussed by application to concentration profiles evolving during the uptake of methanol by the zeolite ferrierite and of methanol by the metal organic framework (MOF) manganese(II) formate. We show that the diffusivity can be calculated most precisely by means of Fick's 1st law. As the circumstances permit, Boltzmann's integration method also yields very precise results. Furthermore, we present a simple procedure that enables the estimation of the influence of the surface barrier on the overall uptake process by plotting the boundary concentration versus the overall uptake.

[1] Author to whom any correspondence should be addressed.

Contents

1. Introduction

Diffusion is one of the most fundamental, omnipresent phenomena in nature and technology. It is especially relevant for nanoporous host particles [1] where the transport properties of the guest molecules are among the crucial features. This is primarily related to their application in separation [2] and catalysis [3] since it is the rate of mass transfer which often decides their technological performance [4, 5].

Many phenomena of (anomalous) mass transfer are caused by the peculiarities of molecules under confinement [6]–[10]. Furthermore, the discrepancies between the results of different measuring techniques [11]–[14] contribute to the continuously increasing interest. The introduction of interference microscopy to study mass transport in nanoporous host systems [15, 16] meant a significant breakthrough because no other technique enables such a detailed view of the concentrations evolving in the crystals.

There exists a large spectrum of techniques able to monitor concentration profiles (e.g. magnetic resonance imaging [17]–[19], positron emission profiling [20] and IR imaging [21]), but only interference microscopy has a spatial resolution in the range of a micrometre. This high

resolution, however, is essential for the observation of intracrystalline concentration profiles within nanoporous crystals with a size of typically 50 μm. Only these transient intracrystalline concentration profiles enable a thorough analysis of mass transport of the guest molecules.

Since the mobility of molecules depends on their mutual interaction, in general, the transport parameters depend on the loading. Under these conditions, macroscopic techniques that are based on an analysis of the time-dependent overall uptake (like gravimetric uptake and release experiments) would fail to provide detailed information on the diffusivity if very large concentration ranges are covered.

In this paper, we present several methods for determining the mass transport parameters, i.e. the transport diffusivity and the surface permeability, from transient intracrystalline concentration profiles. Furthermore, we discuss their application to two different guest–host systems, namely to methanol in the zeolite ferrierite and methanol in the metal organic framework (MOF) manganese(II) formate. Although these systems are fairly different, the efficiency of the respective methods is similar.

2. Experimental

The experimental set-up consists of an optical cell which contains the studied zeolite crystals. The cell is connected to a vacuum system with a vacuum pump and a stock volume of about 2 litres to execute pressure step changes at the beginning of the experiment and to keep the pressure constant at the desired value. The concentration profiles evolving in one single crystal are observed by the interference microscope (section 2.1).

The analysed concentration profiles are monitored during the uptake of pure methanol at room temperature (298 K). In all the experiments considered here, the pressure step is from 0 to 10 mbar.

2.1. Interference microscopy

Figure 1 illustrates the application of interference microscopy to diffusion studies within nanoporous materials. It is based on an analysis of the interference pattern generated by superimposing light beams passing through the nanoporous crystal and the surrounding atmosphere. Since the optical density of the crystal is a function of the concentration of the guest molecules, changes in local concentration directly appear in corresponding changes in the interference pattern (figures 1(b) and (c)). Vice versa, from the interference patterns one may deduce the corresponding concentration profiles (figure 1(d)). The quantity directly accessible is thus the integral over the intracrystalline concentration in the observation direction (the x-axis in figure 1(a)) with a spatial resolution of $\Delta y \times \Delta z \approx 0.5 \times 0.5\,\mu\text{m}^2$. If—due to a corresponding blockage of the relevant crystal faces or by the architecture of the pore system—diffusion in the x-direction is excluded, there is also no concentration variation in the x-direction. In this case, interference microscopy directly yields the local concentrations $c(x, y, z)$.

Interference microscopy cannot provide the absolute values of adsorbate concentration. The absolute concentrations may be calculated with the isotherm available from the literature or measured, for instance, by infrared microscopy. Since the equations describing the transport processes (and therewith the determined transport parameters) are independent of the absolute value of the concentration, in this paper the concentration c is presented in normalized values. This means that the initial concentration is 0 and the final concentration is 1.

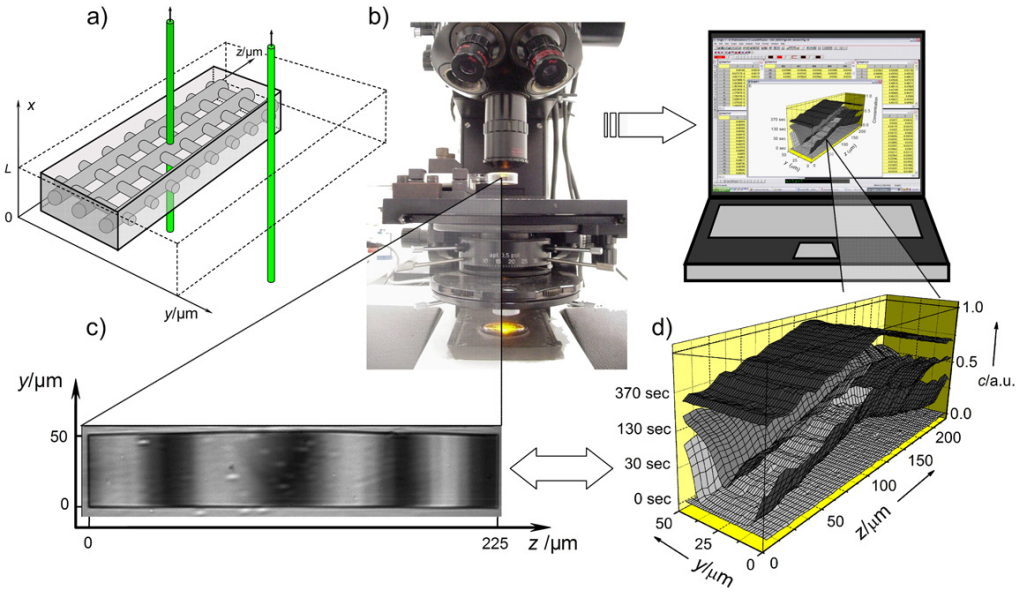

Figure 1. Schematics of interference microscopy. (a) Light beams passing through the crystal and through the surrounding atmosphere. (b) The interference microscope. (c) Interference pattern caused by different optical path lengths. (d) Evolution of the concentration profiles calculated from the interference pattern.

2.2. The investigated nanoporous crystals

The silica–ferrierite zeolite is a cation-free zeolite with two perpendicular channel systems that intersect each other [22]. One channel system is adjusted along the *y*-direction and is framed by an 8-membered ring; this means that they are formed by 8 oxygen and 8 silicon atoms. The other channel system is along the *z*-direction and is formed by 10-membered ring channels. The outer geometry is like a cuboid with its long-side lengths in the *y*- and *z*-directions ($l_y = 25\,\mu$m and $l_z = 100\,\mu$m; l denotes the half-edge length) and a short-side length in the *x*-direction ($l_x = 10\,\mu$m). On both big side faces of the crystal (parallel to *y*–*z*), there are small roof-like parts (figure 2). In previous studies [23, 24] it was found that, due to pore blocking at the channel entrance in the *z*-direction, mass transport essentially proceeds one-dimensionally (1D) (in the *y*-direction). The ferrierite crystals are activated under high vacuum at a temperature of 673 K for 12 h. The activation was preceded by exposing the sample to oxygen at 973 K for 4 h to ensure that there are no organic residues. A gas pressure of 10 mbar causes an equilibrium loading of approximately 1.2 mmol methanol in 1 g zeolite. This corresponds to a relative loading of 30% [24].

The other nanoporous crystal under consideration is manganese(II) formate ($Mn(HCO_2)_2$), a member of the large family of the so-called MOFs [25]. The crystal contains a 1D channel system which is based upon internal cages with a diameter of 0.55 nm (figure 3). The cages are connected by windows with a diameter of 0.45 nm. The crystals are activated under high vacuum at a temperature of 423 K for 24 h. A methanol gas pressure of 10 mbar causes an equilibrium loading of 77 mg methanol in 1 g MOF, which equals a relative loading of 57% [25].

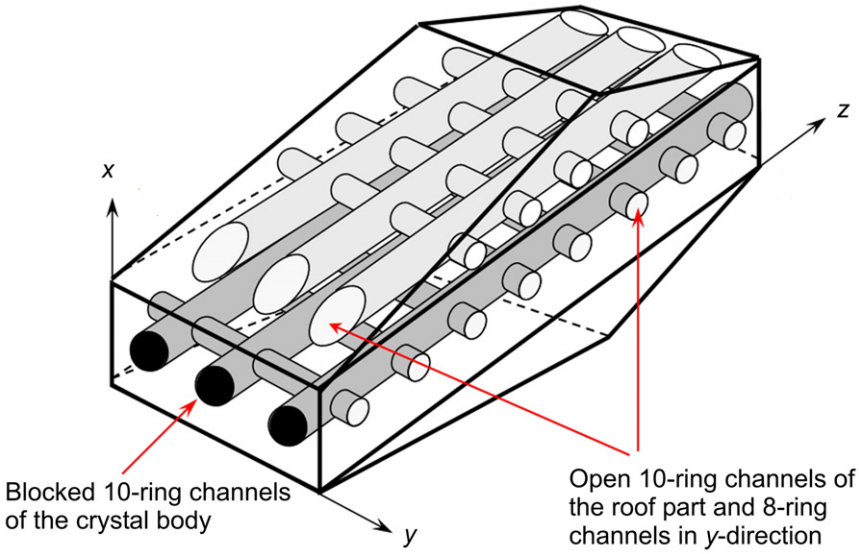

Figure 2. A ferrierite crystal with a 2D pore structure. The scheme shows blocked channels in the *z*-direction in the main body of the crystal, open channels in the *z*-direction in the roof section and open channels in the *y*-direction.

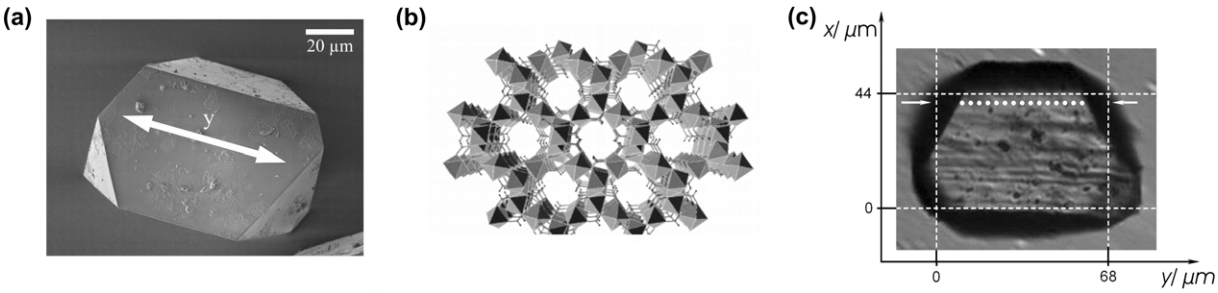

Figure 3. (a) SEM image of a typical MOF manganese(II) formate crystal with the *y*-direction indicated. (b) Scheme of the 1D channel structure. (c) Photograph of the studied crystal, with a dotted line which indicates the crystal part where the analysed profiles have been measured.

3. Mass transport in nanoporous materials

The mass transport of a single-component fluid in a nanoporous host material is already precisely described by the equations derived by Adolf Fick, who observed the proportionality between the flux density j and the gradient of the concentration c. This is known as Fick's 1st law [26, 27] with the transport diffusivity D as a constant of proportionality,

$$j = -D\frac{\partial c}{\partial y}. \tag{1}$$

Since there are no sources or sinks of molecules, conservation of matter,

$$\frac{\partial c}{\partial t} + \frac{\partial j}{\partial y} = 0, \tag{2}$$

is assumed during the diffusion process. The combination of Fick's 1st law with the conservation of matter results in Fick's 2nd law [26],

$$\frac{\partial c}{\partial t} = \frac{\partial}{\partial y}\left(D\frac{\partial c}{\partial y}\right) = D\frac{\partial^2 c}{\partial y^2} + \frac{\partial D}{\partial c}\left(\frac{\partial c}{\partial y}\right)^2. \tag{3}$$

For 3D mass transport, the spatial derivative has to be replaced by the gradient.

Most observed nanoporous crystals [16, 24, 25, 28, 29] exhibit a transport resistance at the surface which hinders the molecules entering the crystal. This effect can be described by [30]

$$j = \alpha(c_{\mathrm{eq}} - c_{\mathrm{surf}}), \tag{4}$$

introducing the surface permeability α as a proportionality factor between the flux density into the crystal and the difference between the actual concentration in the crystal boundary c_{surf} and the equilibrium concentration c_{eq}.

It has been shown [31] that the observed adsorption and desorption processes are essentially isothermal. Therefore, the transport resistance at the crystal surface cannot be explained by non-isothermal effects.

4. Ways of determining the transport diffusivity from intracrystalline concentration profiles

With the obtained concentration profiles and the equations describing the transport process, in principle, the transport diffusivity becomes directly accessible. However, as we will discuss later, the accuracy of the results depends significantly on the method to determine the diffusivity. Furthermore, some methods are subjected to special constraints for their application.

If the mass transport takes place along three directions, the intracrystalline concentration cannot be directly determined from the integrated profiles obtained by interference microscopy. Therefore, a careful recalculation of the intracrystalline concentration profiles needs to be conducted [28]. In general, the non-isotropic mass transport can be best analysed by considering small times when the concentration fronts, which penetrate into the crystal, do not overlap. Therefore, these profiles can be considered as (quasi-) 1D.

In our analysis, we consider the concentration profiles evolving during an adsorption process from 0 to 1. In principle, the following derivations are also valid for desorption (i.e. release) processes.

4.1. Determining the transport diffusivity by Fick's 1st law

The flux density j through an area A corresponds to the amount of molecules diffusing through this area during a time $\mathrm{d}t$, divided by $\mathrm{d}t$ and A. Due to the conservation of matter, the flux density can be calculated by

$$j = \frac{\partial}{\partial t}\int_y^\infty c(y', t)\,\mathrm{d}y'. \tag{5}$$

This can be combined with Fick's 1st law for calculating the transport diffusivity,

$$D(c(y,t)) = -\frac{\frac{\partial}{\partial t}\int_y^\infty c(y', t)\,\mathrm{d}y'}{\partial c/\partial y} \approx -\frac{\int_y^\infty c(y', t+\Delta t)\,\mathrm{d}y' - \int_y^\infty c(y', t)\,\mathrm{d}y'}{\Delta t \cdot \partial c/\partial y}. \tag{6}$$

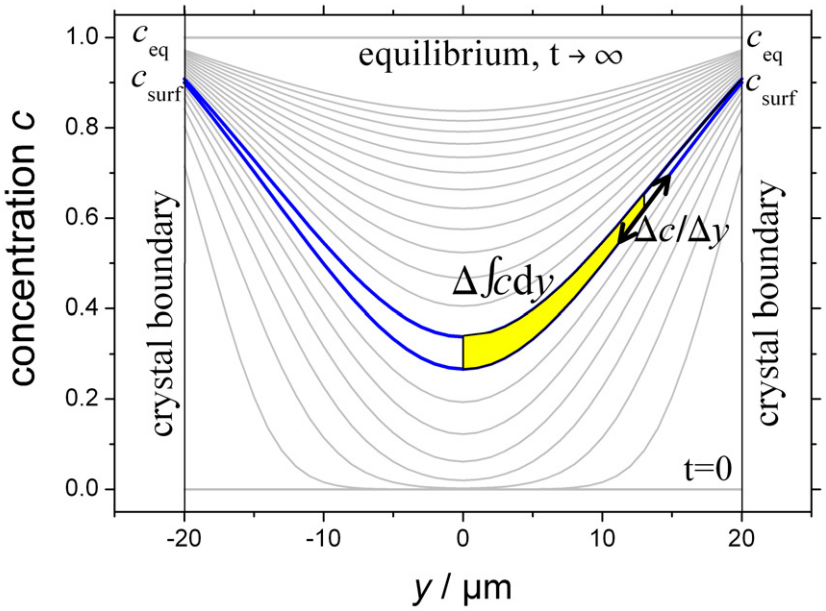

Figure 4. Draft of the application of Fick's 1st law. The change in the overall uptake and the spatial derivative are shown. Furthermore, the boundary concentration c_{surf} and the equilibrium concentration c_{eq} are marked.

In 1D systems wherein the uptake or release proceeds from two opposite faces ($y = -l$ and $y = l$), due to symmetry, the upper limit of integration is replaced by the y-value in the centre ($y = 0$).

Consequently, two succeeding concentration profiles enable the calculation of the concentration-dependent transport diffusivity for the entire concentration range covered by the concentration profiles. The application is sketched in figure 4.

4.2. Determining the transport diffusivity by Fick's 2nd law

In the centre of the concentration profile, the first spatial derivative of the concentration is 0 due to symmetry. Therefore, Fick's 2nd law (equation (3)) can be directly used for determining the transport diffusivity in the centre [23] (figure 5),

$$D_{\text{centre}} = \frac{\partial c/\partial t}{\partial^2 c/\partial y^2}. \tag{7}$$

The thus determined diffusivity can be used in equation (3) for calculating the diffusivity outside of the centre,

$$D = \frac{\partial c/\partial t}{\partial^2 c/\partial y^2} - \frac{(\partial D'/\partial c)\,(\partial c/\partial y)^2}{\partial^2 c/\partial y^2}. \tag{8}$$

If the concentration profiles are very precise, equation (8) can also be used in an iterative way.

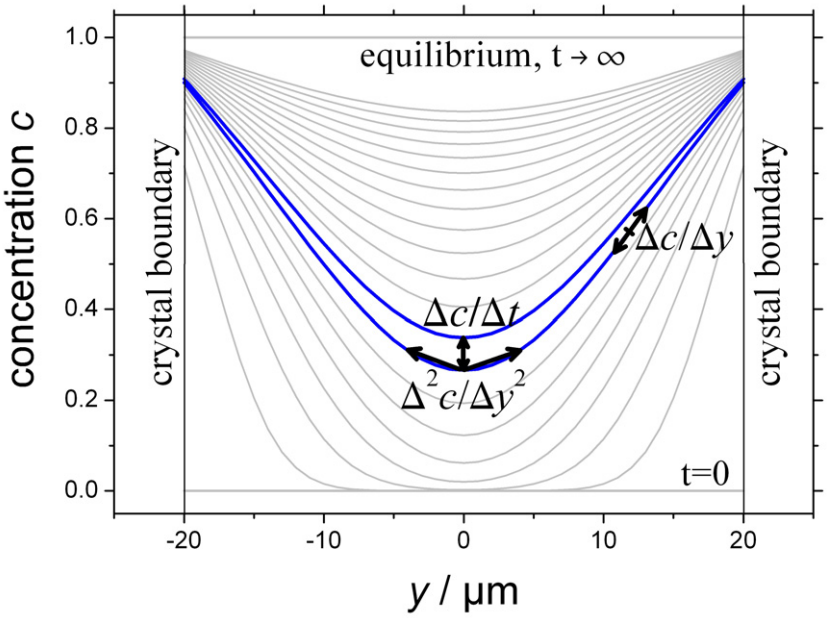

Figure 5. Draft of the application of Fick's 2nd law. The temporal and the second spatial derivative are shown in the centre. The first spatial derivative is shown beyond the centre.

4.3. Determining the transport diffusivity by means of Boltzmann's integration method

A particularly elegant means to deduce diffusivities from transient 1D concentration profiles is presented by Boltzmann's integration method [32, 33]. However, for applying this method, the following conditions must be fulfilled:

(i) the initial concentration is uniform all over the crystal ($c(y, t = 0) = c_0$);

(ii) the evolution of the transient concentration profiles is initiated by a step change in the boundary concentration which, later on, remains constant ($c(y = 0, t) = c_{eq}$); and

(iii) the time interval considered is small enough so that the diffusion front evolving from one side has not yet reached the opposite one. Therefore, the systems may be considered to be semi-infinitely extended ($c(y = \infty, t) = c_0$).

By introducing a new variable $\eta = y/\sqrt{t}$, Fick's 2nd law (equation (3)) transforms to

$$\frac{\mathrm{d}}{\mathrm{d}\eta}\left(D\frac{\mathrm{d}c}{\mathrm{d}\eta}\right) = -\frac{\eta}{2}\frac{\mathrm{d}c}{\mathrm{d}\eta}. \tag{9}$$

Integration over this equation over η from ∞ to $\eta(c)$ with $\mathrm{d}c/\mathrm{d}\eta|_{\eta=\infty} = 0$ yields

$$D(c) = -\frac{1}{2}\frac{\mathrm{d}\eta}{\mathrm{d}c}\int_{c=c_0}^{c}\eta\,\mathrm{d}c = -\frac{1}{2t}\frac{\mathrm{d}y}{\mathrm{d}c}\int_{c=c_0}^{c} y\,\mathrm{d}c. \tag{10}$$

In this way, the diffusivity at any concentration $c_0 < c < c_{eq}$ covered during the whole process of uptake or release may simply be determined from the respective integral $\int_{c=c_0}^{c} y\,\mathrm{d}c$ and its slope $\mathrm{d}y/\mathrm{d}c$ at the given concentration (figure 6). Therefore, one concentration profile obtained

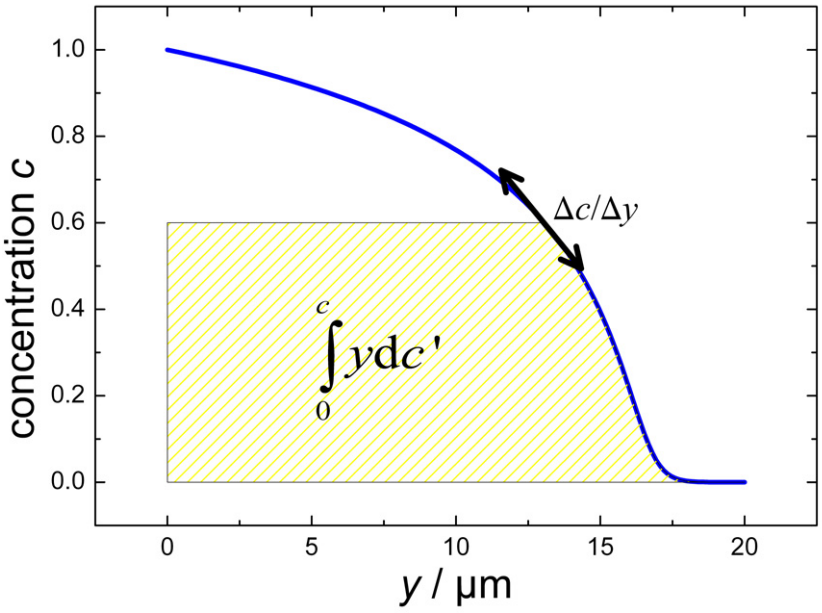

Figure 6. Draft of the application of Boltzmann's integration method. The spatial derivative of the concentration and the concentration integral are shown.

at one single point in time is sufficient to analyse the whole concentration dependence of the diffusivity.

In most applications a surface barrier is found [24, 25, 28, 29] which hinders the mass transport at the crystal margins; this means that condition (ii) is not fulfilled. If the influence of the surface barrier is not too large, this means that if the concentration at the crystal boundary is not too small ($c_{\mathrm{bound}} \gtrsim 0.5 c_{\mathrm{eq}}$), this influence can be corrected by a virtual enlargement of the concentration profiles [34, 35].

4.4. Solving Fick's 2nd law as a first-order linear differential equation

By dividing equation (3) by $(\partial c/\partial y)^2$, Fick's 2nd law can be transformed to

$$a(c) = D(c) \cdot b(c) + \frac{\partial D}{\partial c} \tag{11}$$

with

$$a(c) = \frac{\partial c/\partial t}{(\partial c/\partial y)^2} \qquad \text{and} \qquad b(c) = \frac{\partial^2 c/\partial y^2}{(\partial c/\partial y)^2}. \tag{12}$$

Equation (11) is a first-order linear differential equation which can be generally solved [36] to

$$D(c) = \exp\left(-\int b\,\mathrm{d}x\right)\left[\int a\,\exp\left(\int b\,\mathrm{d}x\right)\mathrm{d}x + C\right] \tag{13}$$

with C as a constant of integration. Equation (13) can be rewritten as

$$D(c) = \exp\left(-\int \frac{\partial^2 c/\partial y^2}{(\partial c/\partial y)^2}\,\mathrm{d}x\right)\left[\int \frac{\partial c/\partial t}{(\partial c/\partial y)^2}\exp\left(\int \frac{\partial^2 c/\partial y^2}{(\partial c/\partial y)^2}\,\mathrm{d}x\right)\mathrm{d}x + D(c_0)\right]. \tag{14}$$

Thus, the diffusivity may be calculated from the spatial and temporal dependence of the concentration profiles (see figure 5). As a significant drawback the diffusivity at the initial concentration, $D(c_0)$, has to be known as an integration constant [37].

4.5. Fitting the concentration profiles with a finite difference solution of Fick's 2nd law

A very general method is the calculation of the concentration profiles evolving during the uptake or release process with given transport parameters. The calculation can be performed by a finite difference solution of Fick's 2nd law [30] (see the supplement). Beginning with the initial conditions at $t = 0$, this algorithm successively calculates the concentration profiles for every time step Δt (Δt is typically much smaller than 1 s). By varying the assumed diffusivity and calculating the standard deviation between the calculated and the measured concentration profiles, the diffusivity describing the transport process can be determined.

This method is not limited to 1D. Therefore, concentration profiles evolving during 2D or 3D mass transport can also be analysed [28, 38]. However, this method requires a lot of computing time (roughly 1 min for a 1D uptake process, depending on the resolution).

5. Determining the surface permeability of the crystal

The surface permeability α can be determined with equation (4),

$$\alpha = \frac{j}{c_{\mathrm{eq}} - c_{\mathrm{surf}}}. \tag{15}$$

The flux density j may be determined most powerfully by considering the number of molecules that have penetrated through the surface by using equation (5) (see figure 4, with integration limits at the centre and at the crystal boundary). In principle, the flux density can also be approximated by equation (1) near the surface. However, to achieve reasonable results, this method requires an extremely high accuracy of the measured concentration profiles. The sticking probability, which gives the probability that a gas molecule hitting the surface continues its trajectory into the crystal, can be calculated from the thus determined surface permeability [41].

6. Estimating the influence of the surface resistance on the overall uptake or release process

A powerful tool for determining the influence of the surface resistance on the overall transport process is provided by plotting the concentration at the crystal boundary $c_{\mathrm{surf}}(t)$ versus the overall uptake $m(t)$ [39] (figure 7).

Assuming a constant transport diffusivity D and a constant surface permeability α, during molecular uptake the normalized concentration profile within a host particle of length $2l$ is given by the relation [30]

$$c(y, t) = 1 - \sum_{n=1}^{\infty} \frac{2L \cos(\beta_n y/l) \exp\left(-\beta_n^2 Dt/l^2\right)}{\left(\beta_n^2 + L^2 + L\right) \cos \beta_n}, \tag{16}$$

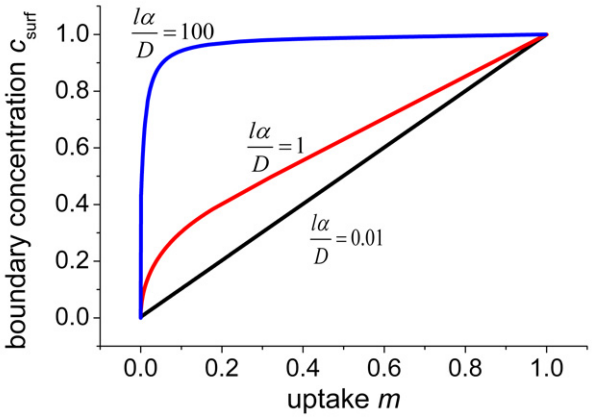

Figure 7. Correlation between the actual boundary concentration c_{surf} and the uptake m at the corresponding instant of time. Three different cases are shown: the mass transport is essentially limited by intracrystalline diffusion ($l\alpha/D = 100$), by surface barriers ($l\alpha/D = 0.01$) and both by intracrystalline diffusion and surface resistance ($l\alpha/D = 1$).

where the β_{n}s are the positive roots of

$$L = \frac{l\alpha}{D} = \beta_n \tan \beta_n. \tag{17}$$

Integration over the system in the diffusion (i.e. y-) direction from $-l$ to l yields

$$m(t) = 1 - \sum_{n=1}^{\infty} \frac{2L^2 \exp\left(-\beta_n^2 Dt/l^2\right)}{\left(\beta_n^2 + L^2 + L\right)\beta_n^2} \tag{18}$$

for the overall uptake at time t. In the long-time limit (i.e. only considering the first summand), the combination of equation (18) with (16) at $y = -l$ or l yields

$$c_{\mathrm{surf}}(t) = c(y = l, t) = 1 - \frac{\beta_1^2}{L} + \frac{\beta_1^2}{L} \cdot m(t). \tag{19}$$

Thus, the intercept w of the asymptote of the c_{surf}–m correlation plot to the ordinate is found to be given by the relation

$$w = 1 - \frac{\beta_1^2}{L}. \tag{20}$$

In a qualitative way, the reciprocal value of this intercept, w^{-1}, is expected to indicate the relevance of surface barriers to the overall process of molecular exchange.

The time constant of an uptake process [30] controlled only by diffusion is

$$\tau_{\mathrm{diff}} = \int_0^{\infty} (1 - m(t))\, \mathrm{d}t = \frac{l^2}{3D}. \tag{21}$$

If there is an additional surface barrier, the time constant can be calculated to be

$$\tau_{\mathrm{surf+diff}} = \int_0^{\infty} (1 - m(t))\, \mathrm{d}t = \frac{l^2}{3D} + \frac{l}{\alpha}. \tag{22}$$

Therefore, the ratio of the quotient of the exchange times (equations (21) and (22)) to the reciprocal value of w can be reformulated as

$$\frac{\tau_{\text{surf+diff}}/\tau_{\text{diff}}}{w^{-1}} = \left(1+\frac{3}{L}\right)\left(1-\frac{\beta_1^2}{L}\right) = 1+\frac{3\cdot\tan\beta_1/\beta_1-\beta_1\cdot\tan\beta_1-3}{\tan^2\beta_1}, \tag{23}$$

which comes out to be between 1 and 1.052 for β_1 varying in the range of 0 to $\pi/2$ (corresponding to a variation of $L = l\alpha/D = \beta_1\cdot\tan\beta_1$ between 0 and ∞, i.e. over all possible values). Therefore, the reciprocal value of the intercept of the extrapolated linear part of the c_{surf}–m correlation plot may be taken as an estimate of the factor by which the presence of the surface barrier leads to a prolongation of molecular uptake.

The demonstrated equivalence of the ratio of the exchange times $\tau_{\text{surf+diff}}/\tau_{\text{diff}}$ and the reciprocal value of the intercept w^{-1} (equation (23)) implies concentration-independent transport parameters. In real systems, however, the transport diffusivity as well as the surface permeability may depend on concentration. It is shown in [40] that even for concentration-dependent transport diffusion and surface permeation as well as for 3D mass transport in a cuboid, $\tau_{\text{surf+diff}}/\tau_{\text{diff}}$ equals w^{-1}.

7. Determining the transport parameters from profiles measured by interference microscopy

The methods explained in sections 4 and 5 can be applied to concentration profiles obtained by interference microscopy. To average the inherent scattering of every single concentration value, a concentration profile obtained at time t is fitted by the following term:

$$c_{\text{fit};t}(x) = \sum_{n=0}^{n_{\max}} a_n \cos\left(n\frac{x-l}{l}\right). \tag{24}$$

This term, which perfectly fits every single concentration profile, is used for further analyses ($n_{\max}$ is generally set as 10).

This smoothing method and the imperfections of the data may cause an oscillation of the results. However, this oscillation has a much smaller magnitude than the scattering from the unsmoothed data.

For quantization of the accuracy of the corresponding method, we calculate the relative standard deviation referring to the mean concentration dependence,

$$\sigma_{\text{rel}} = \frac{\sqrt{\frac{1}{n}\sum_n (D_{\text{mean}}-D)^2}}{D_{\text{mean}}} = \sqrt{\frac{1}{n}\sum_n \left(1-\frac{D(c)}{D_{\text{mean}}(c)}\right)^2}. \tag{25}$$

$D_{\text{mean}}(c)$ denotes the mean diffusivity (n is the number of data points).

7.1. Methanol in ferrierite

We studied the adsorption of methanol in the zeolite ferrierite [24]. Due to the blocking of the entrances to the pores along the z-direction, the mass transport proceeds essentially along the y-direction. As shown in [24], the influence of the diffusion along the z-direction increases with increasing pressure step. Hence, we analyse the uptake process for a gas-phase pressure step from 0 to 10 mbar which (almost completely) proceeds one dimensionally. The concentration

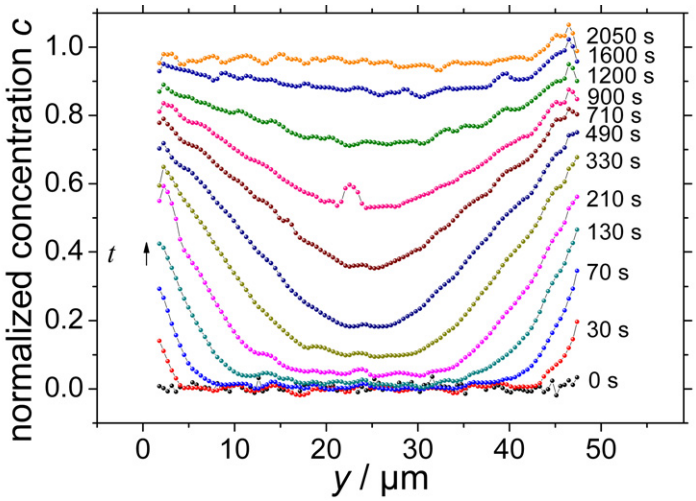

Figure 8. Normalized concentration profiles of methanol in the crystal body of ferrierite (along the *y*-direction) [24]. The gas pressure step is from 0 to 10 mbar.

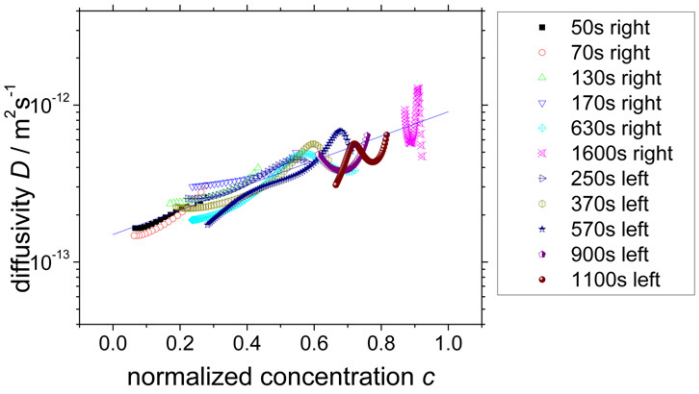

Figure 9. Diffusivity of methanol in ferrierite determined by means of Fick's 1st law. The results can be described with $D = 1.5\exp(1.8c) \times 10^{-13}\,\mathrm{m^2\,s^{-1}}$ (thin line) with a relative standard deviation of 17%.

profiles evolving in the body of the crystal are pictured in figure 8. These profiles are curved, which shows the important influence of the transport diffusion resistance. Furthermore, the concentration at the crystal boundary has not immediately reached the equilibrium value due to the transport resistance at the crystal surface.

The transport diffusivities calculated with Fick's 1st law (equation (6)) are shown in figure 9. The results determined from different profile branches and determined at different times show very good agreement. The transport diffusivity was found to be approximately $1.5\exp(1.8c) \times 10^{-13}\,\mathrm{m^2\,s^{-1}}$ with a relative standard deviation of 17%.

The results of Fick's 2nd law are shown in figure 10. The diffusivity determined in the centre can also be described with $1.5\exp(1.8c) \times 10^{-13}\,\mathrm{m^2\,s^{-1}}$; however, the scattering of the single results is significant ($\sigma_{\mathrm{rel}} = 61\%$). This dependency can be used in equation (8) for calculating the diffusivity in the entire concentration profile. These diffusivities, calculated beyond the centre, also exhibit substantial scattering ($\sigma_{\mathrm{rel}} = 101\%$). It is noteworthy that the

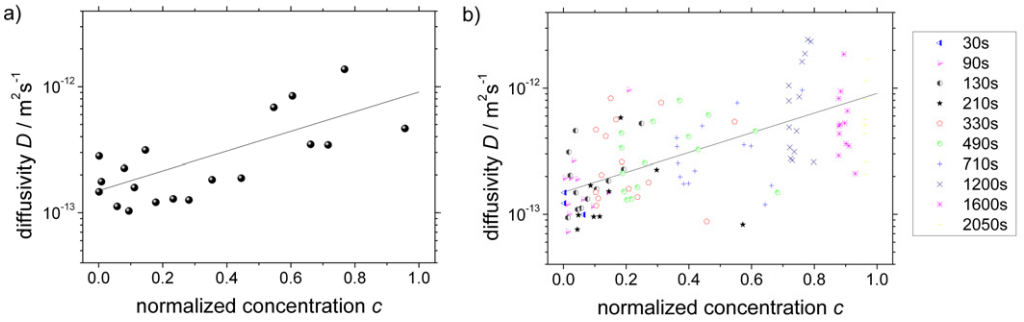

Figure 10. Diffusivity of methanol in ferrierite determined by Fick's 2nd law ((a) in the centre; (b) over the entire profile). The relative standard deviations appear to be 61% (a) and 101% (b), respectively.

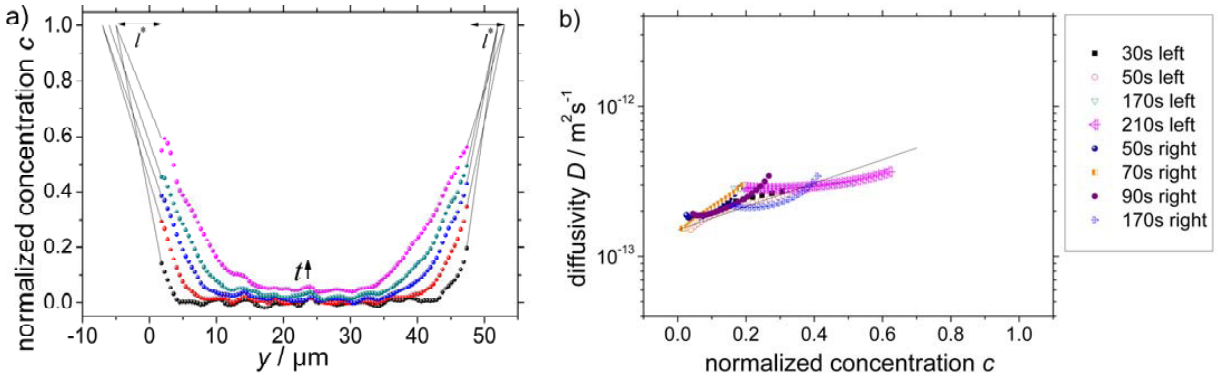

Figure 11. Application of Boltzmann's integration method. (a) Concentration profiles extended by a certain length l^* to eliminate the influence of the surface barrier ($t = 30$–210 s). (b) The resulting diffusivity with a relative standard deviation of 19% referring to $D = 1.5 \exp(1.8c) \times 10^{-13}\,\mathrm{m^2\,s^{-1}}$.

large value of the standard deviation is mainly caused by values larger than the mean diffusivity and the distribution of the results is not symmetrical.

The application of Boltzmann's integration method is limited to semi-infinite concentration profiles. Therefore, only small times ($t < 230$ s) can be considered when the concentration fronts penetrating from the opposing crystal faces do not yet overlap. Furthermore, the existence of a surface barrier hinders the direct application of Boltzmann's integration method to the concentration profiles. Therefore, we have to extend the concentration profiles imaginarily (by a certain length l^* to correct for the surface barrier (figure 11(a))). This can be done simply by extending the profiles with the slope at the margins. The extended profiles have (approximately) the shape of only diffusion-controlled concentration profiles. These profiles enable the calculation of the transport diffusivities with Boltzmann's integration method (figure 11(b)). The results are in very good agreement with previous ones and show a small scattering ($\sigma_{\mathrm{rel}} = 19\%$). However, due to the reduced boundary concentration, the diffusivity can be calculated only for concentrations smaller than 0.6.

For using the standard solution of a first-order linear differential equation, we have to know the diffusivity at any concentration (best at the initial concentration). With the diffusivity

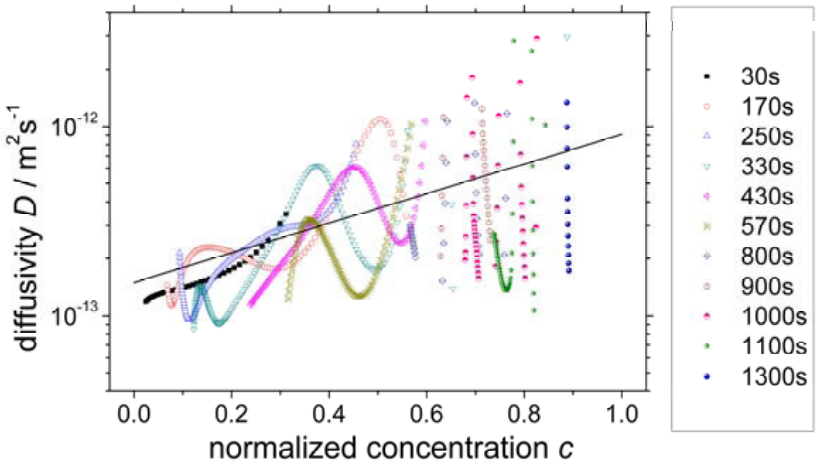

Figure 12. Diffusivity of methanol in ferrierite determined with the standard solution of a linear differential equation (equation (14); thin line: $D = 1.5\exp(1.8c) \times 10^{-13}\,\mathrm{m^2\,s^{-1}}$, $\sigma_{\mathrm{rel}} = 160\%$).

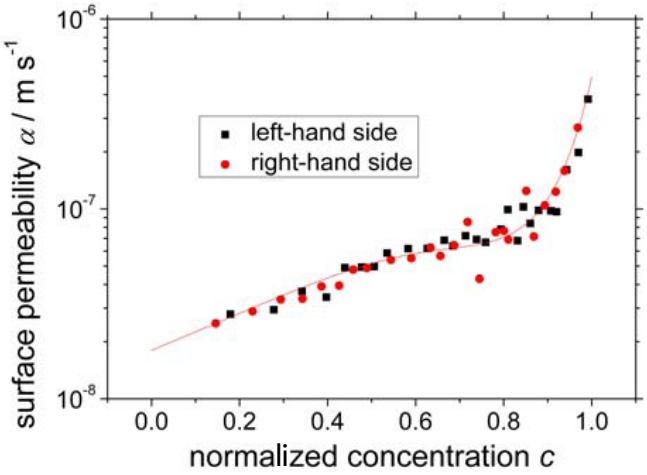

Figure 13. Surface permeability determined with equation (15). The results can be well described with $\alpha = 1.8\exp(2.246c - 6.4c^6 + 7.47c^8) \times 10^{-8}\,\mathrm{m\,s^{-1}}$ (black line).

determined by other methods ($1.5\exp(1.8c) \times 10^{-13}\,\mathrm{m^2\,s^{-1}}$), this standard solution results in transport diffusivities that scatter significantly (figure 12; $\sigma_{\mathrm{rel}} = 160\%$).

The surface permeability can be determined very precisely with equation (15) (figure 13). Both sides of the concentration profiles yield essentially identical results. It is found that the surface permeability increases by more than one order of magnitude in the considered concentration range ($\alpha = 1.8\exp(2.246c - 6.4c^6 + 7.47c^8) \times 10^{-8}\,\mathrm{m\,s^{-1}}$).

If we plot the boundary concentration versus the overall uptake by the crystal, we can determine the relative influence of the surface barrier (figure 14). The intersection of the asymptote and the ordinate results to be about 0.56 for both sides of the concentration profile. This corresponds to a factor of 1.8 by which the transport process is retarded due to the transport

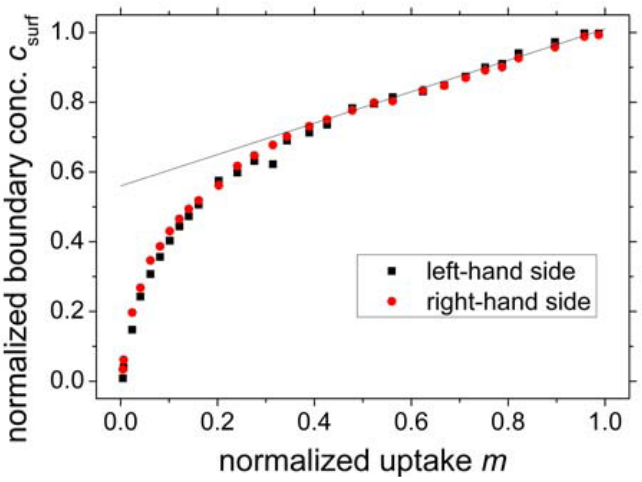

Figure 14. Boundary concentration as a function of the overall uptake. The intersection of the ordinate and the asymptote yields 0.56.

resistance at the surface. With a mean surface permeability of $7.5 \times 10^{-8}\,\mathrm{m\,s^{-1}}$ and a mean diffusivity of $4.2 \times 10^{-13}\,\mathrm{m^2\,s^{-1}}$, we estimate that the transport process is retarded by a factor of 1.7 due to the surface resistance. This is in good agreement with the value determined by the c_{surf}–m plot.

The validity of the above-determined transport parameters can be verified by means of the numerical solution of Fick's 2nd law. The measured profiles are approximated very well by assuming a transport diffusivity of $1.5\exp(1.8c) \times 10^{-13}\,\mathrm{m^2\,s^{-1}}$ and a surface permeability of $1.8\exp(2.246c - 6.4c^6 + 7.47c^8) \times 10^{-8}\,\mathrm{m\,s^{-1}}$. The standard deviation results to be 3.4%.

The other way around, the transport diffusivity and the surface permeability were set as ninth-order polynomials. By varying the factors with a genetic algorithm, the profiles can be fitted very well (with $D = (160 + 380.4c + 11.3c^2 + 8.8c^3 + 6.1c^4 + 5.5c^5 + 6.7c^6 + 4.8c^7 + 1.1c^8 + 6.2c^9) \times 10^{-15}\,\mathrm{m^2\,s^{-1}}$ and $\alpha = (2.442 + 0.123c + 9.249c^2 + 0.069c^3 + 1.349c^4 + 0.314c^5 + 1.252c^6 + 0.903c^7 + 0.113c^8 + 4.044c^9) \times 10^{-8}\,\mathrm{m\,s^{-1}}$). The standard deviation between the measured and the simulated concentration profiles results to be 2.9%. These values resemble the values used above (diffusivity, $\sigma_{rel} = 16\%$, and surface permeability, $\sigma_{rel} = 22\%$). This method consumes a lot of computing time since the genetic algorithm has to calculate the concentration profiles for at least 1000 parameter sets to reach a reasonable accuracy. (Even with a low resolution, a modern personal computer needs several hours or days!)

7.2. Methanol in the MOF manganese(II) formate

In the MOF manganese(II) formate, there exists only a 1D channel system. The monitored concentration profiles, which are obtained at the dotted line in figure 3(c) are shown in figure 15. These profiles are curved, indicating the important influence of the transport diffusion resistance. Furthermore, due to the surface barrier, the concentration at the crystal boundary does not immediately reach the equilibrium value. The concentration profiles do not show perfect symmetry, which is caused by the complex outer geometry (additionally, maybe, by some crystal defects).

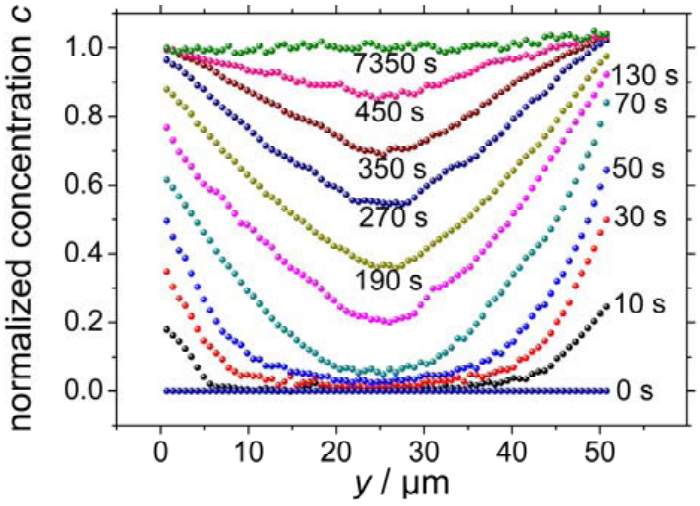

Figure 15. Normalized concentration profiles of methanol in the MOF manganese(II) formate determined at the dotted line in figure 3(c) [25]. The gas pressure step is from 0 to 10 mbar.

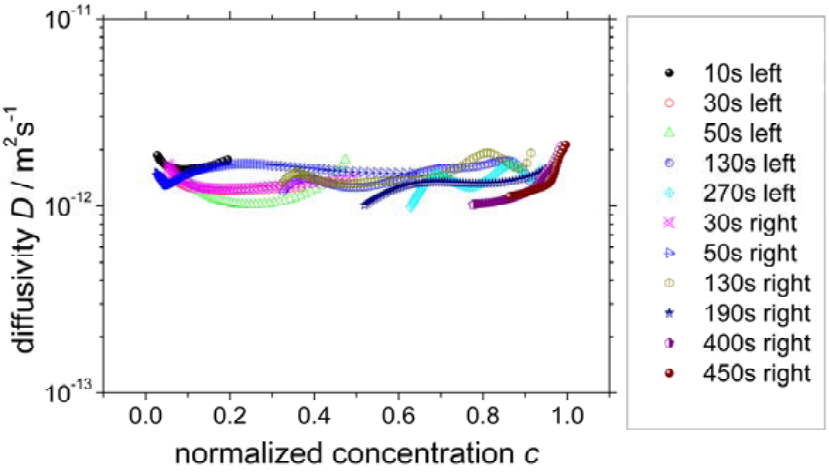

Figure 16. Diffusivity of methanol in the MOF manganese(II) formate determined by Fick's 1st law. The results are constant, with a mean value of $1.45 \times 10^{-12}\,\mathrm{m^2\,s^{-1}}$ and a relative standard deviation of 18%.

The results of the method directly derived from Fick's 1st law (equation (6)) are shown in figure 16. The diffusivities determined at several times in both sides of the concentration profiles show very good agreement. The thus determined diffusivity is (approximately) constant ($D = 1.45 \times 10^{-12}\,\mathrm{m^2\,s^{-1}}$; $\sigma_{\mathrm{rel}} = 18\%$).

Applying Fick's 2nd law yields similar diffusivities (figure 17). The diffusivities determined in the centre of the concentration profiles (equation (7)) are essentially constant ($D = 1.75 \times 10^{-12}\,\mathrm{m^2\,s^{-1}}$; $\sigma_{\mathrm{rel}} = 43\%$). This can be used in equation (8) for determining the diffusivity in the entire crystal range ($D = 1.77 \times 10^{-12}\,\mathrm{m^2\,s^{-1}}$; $\sigma_{\mathrm{rel}} = 80\%$).

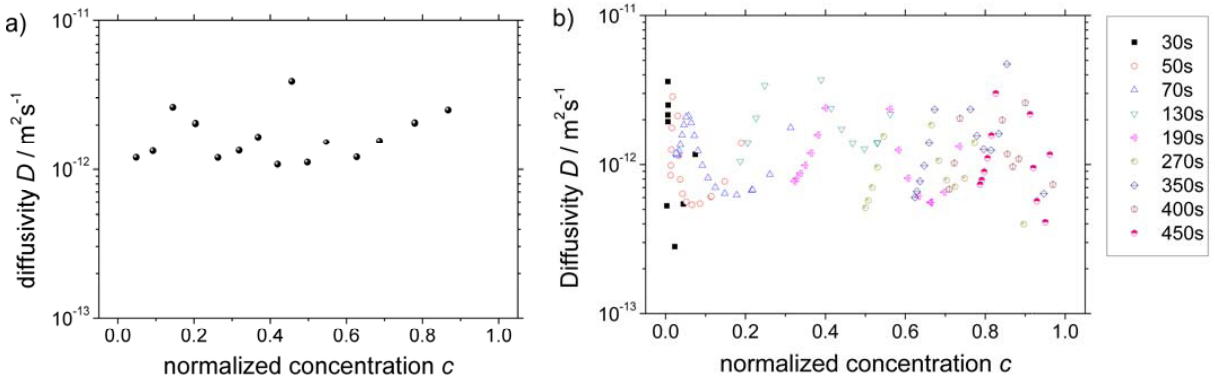

Figure 17. Diffusivity of methanol in the MOF manganese(II) formate determined by Fick's 2nd law ((a) in the centre; (b) over the entire profile). The mean values are $1.75 \times 10^{-12}\,m^2\,s^{-1}$ (a; with a relative standard deviation of 43%) and $1.77 \times 10^{-12}\,m^2\,s^{-1}$ (b; with a relative standard deviation of 80%), respectively.

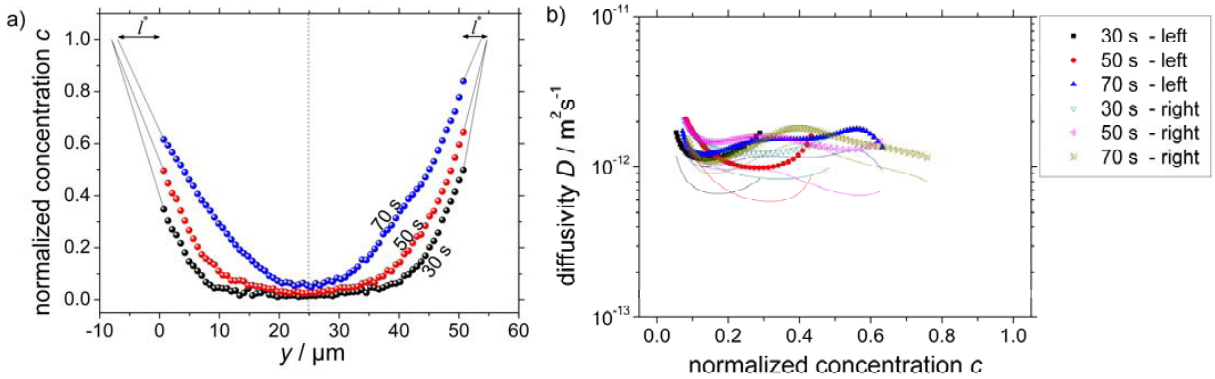

Figure 18. Application of Boltzmann's integration method. (a) Concentration profiles of methanol in the MOF manganese(II) formate extended by a certain length l^* to eliminate the influence of the surface barrier. (b) The resulting diffusivity with a mean value of $1.38 \times 10^{-12}\,m^2\,s^{-1}$ and a relative standard deviation of 15%. The uncorrected results (without correcting the surface barrier) are plotted as thin lines.

The application of Boltzmann's integration method is limited to concentration profiles obtained at times $t < 90$ s, when the concentration fronts penetrating from the opposing crystal faces do not yet overlap. Furthermore, we have to correct for the influence of the surface barrier by extending the concentration profiles imaginarily (by length l^*, figure 18(a)). The extended profiles enable the calculation of the transport diffusivities with Boltzmann's integration method (figure 18(b)). These results are in very good agreement with the previous ones and show a very small scattering ($D = 1.38 \times 10^{-12}\,m^2\,s^{-1}$; $\sigma_{rel} = 15\%$).

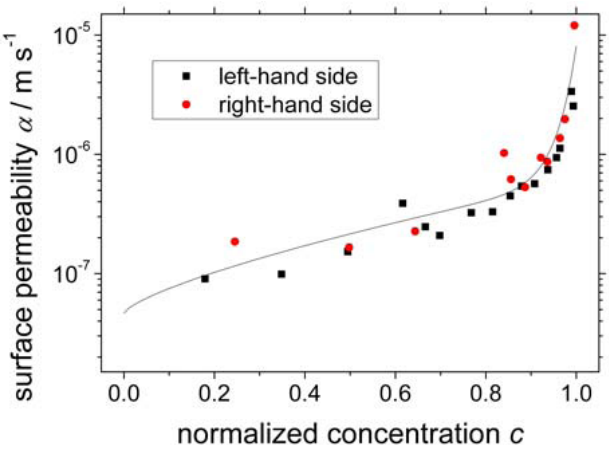

Figure 19. Surface permeability determined with equation (15). The results can be well described with $\alpha = 4.67\exp(2.53c^{0.727} + 2.62c^{21.52}) \times 10^{-8}\,\mathrm{m\,s^{-1}}$ (black line).

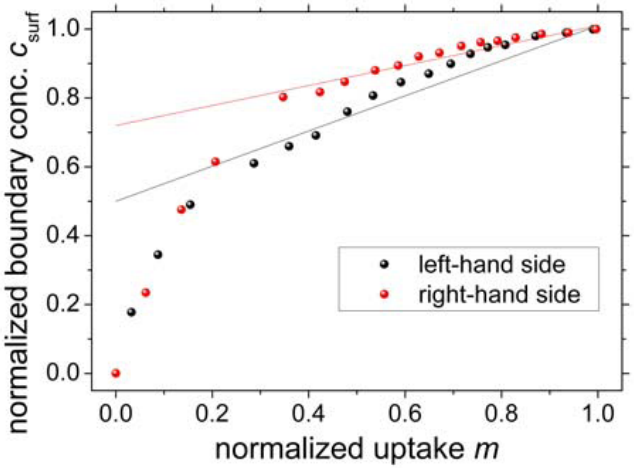

Figure 20. Boundary concentration as a function of the overall uptake. The intersections of the ordinate and the asymptote yield 0.5 and 0.72, respectively.

Assuming $D_0 = 1.45 \times 10^{-12}\,\mathrm{m^2\,s^{-1}}$, the standard solution of a first-order linear differential equation yields a transport diffusivity which is approximately $1.5 \times 10^{-12}\,\mathrm{m^2\,s^{-1}}$, but shows a high scattering ($\sigma_{\mathrm{rel}} = 69\%$).

The surface permeability α (determined by equation (15)) increases significantly over the considered concentration range ($\alpha = 4.67\exp(2.53c^{0.727} + 2.62c^{21.52}) \times 10^{-8}\,\mathrm{m\,s^{-1}}$; figure 19).

In the plot of the boundary concentration versus the overall uptake, the intersection of the asymptote and the ordinate amounts to about 0.61. (This is the mean value of 0.50 at the left-hand crystal side and 0.72 at the right-hand crystal side (figure 20).) This corresponds to a factor of 1.6 by which the transport process is retarded due to the transport resistance at the surface. With a mean surface permeability of $4 \times 10^{-7}\,\mathrm{m\,s^{-1}}$ (geometrical mean of all calculated α) and a

diffusivity of $1.45 \times 10^{-12}\,m^2\,s^{-1}$, we calculate that the transport process is retarded by a factor of 1.45 due to the surface resistance. This is in good agreement with the value determined by the c_{bound}–m plot.

These transport parameters are verified by the numerical solution of Fick's 2nd law. With a transport diffusivity $D = 1.45\exp(1.8c) \times 10^{-13}\,m^2\,s^{-1}$ and a surface permeability $\alpha = 4.67\exp(2.53c^{0.727} + 2.62c^{21.52}) \times 10^{-8}\,m\,s^{-1}$, the standard deviation between the measured and calculated profiles results to be 3.6%.

On the other hand, setting the diffusivity and the surface permeability as a ninth-order polynomial, the standard deviation appears to be 3.4% ($D = (148.4 + 0.01c + 0.001c^2 + 0.009c^3 + 0.01c^4 + 0.01c^5 + 0.006c^6 + 0.01c^7 - 0.01c^8 - 0.008c^9) \times 10^{-14}\,m^2\,s^{-1}$ and $\alpha = (9.88 + 3.49c - 5.16c^2 + 79.14c^3 - 42.04c^4 + 85.30c^5 + 48.61c^6 - 323.04c^7 - 49.7c^8 + 351.2c^9) \times 10^{-8}\,m\,s^{-1}$). These values are in good agreement with the transport parameters calculated above (diffusivity, $\sigma_{rel} = 2.5\%$, and surface permeability, $\sigma_{rel} = 33\%$).

8. Discussion of the different methods

In the previous sections, we have considered five different ways to determine the transport diffusivity from transient, intracrystalline concentration profiles. The most important features of the methods are the requirements for their application and the precision of data analysis. The latter may, potentially, compensate for shortcomings in the quality of the primary data, i.e. for low signal-to-noise ratios of the measured concentrations. The highest data precision is provided by the procedure based on Fick's 1st law (equation (6)) and Boltzmann's integration method (equation (10)). The results of Fick's 1st law show very low scattering (the relative standard deviations are 17 and 18%, respectively). Furthermore, the application of equation (6) does not require any boundary conditions. However, if the temporal resolution of the profiles is rather poor, the quality of the results of this method dramatically declines. Since interference microscopy enables a temporal resolution up to 10 s, transport processes with a time constant of more than 100 s can be thoroughly analysed by Fick's 1st law.

If there exist no surface barriers, Boltzmann's integration method is also very powerful. However, in most of the systems studied previously, such barriers were observed. Small transport resistances at the surface can be corrected, however, by elongating the concentration profiles. As the most significant advantage of this very precise method ($\sigma_{rel} = 19$ and 15%, respectively), a single concentration profile obtained at a certain instant of time is sufficient for calculating the whole concentration dependence of the diffusivity. However, due to the limitation to semi-infinite profiles, only concentration profiles obtained at small times can be considered. Thus, the determination of the whole concentration dependence is often hampered by the existence of the surface barriers which retard the equilibration of the boundary concentration. In both examples, the diffusivities can only be calculated up to a normalized concentration of approximately 0.6 and 0.8, respectively.

The results of the direct (differential) application of Fick's 2nd law (equations (7) and (8)) and the application of the standard solution of Fick's 2nd law transformed to a first-order linear differential equation (equation (14)) exhibit a poor accuracy compared to previous methods. This is a consequence of the high uncertainty of the second spatial derivative of the concentration. As a further disadvantage, application of equation (14) implies knowledge of the diffusivity at a certain concentration. The advantage of the direct application of Fick's 2nd law is its simplicity. No integration is needed, so it is very fast, without requiring much computing time.

If there is enough computing time available, the transport parameter can also be very well estimated indirectly by using the finite difference solution of Fick's 2nd law. The thus obtained functions for the transport diffusivity and the surface permeability were found to be in very good agreement with the results of the other methods. Although this method is pretty slow, its application is recommended to verify the validity of already determined transport diffusivities. Furthermore, this procedure also enables the estimation of the surface permeability.

The surface permeability can also be calculated directly by considering the flux through the surface and the difference between the actual and equilibrium surface concentrations. This method is very precise and has similarities to the method based on Fick's 1st law.

We determined the transport diffusivity of methanol in ferrierite in the y-direction to be $1.5\exp(1.8c) \times 10^{-13}\,\mathrm{m^2\,s^{-1}}$ and of methanol in the MOF manganese(II) formate to be $1.45 \times 10^{-12}\,\mathrm{m^2\,s^{-1}}$. Thus, with increasing concentration, the transport diffusivity in ferrierite increases by a factor of 6, whereas in the MOF crystal it is constant.

The determined surface resistances are strongly dependent on the concentration. In both examples, the surface permeability ($\alpha_{\mathrm{Ferr}} = 1.8\exp(2.246c - 6.4c^6 + 7.47c^8) \times 10^{-8}\,\mathrm{m\,s^{-1}}$ and $\alpha_{\mathrm{MOF}} = 4.67\exp(2.53c^{0.727} + 2.62c^{21.52}) \times 10^{-8}\,\mathrm{m\,s^{-1}}$) increases by more than one order of magnitude. This non-constant surface permeability prohibits analysis using the analytical solutions of the diffusion equation [30], even if the diffusivity is constant.

The relevance of the surface resistances to the overall mass transfer may most easily be revealed by plotting the boundary concentration c_{surf} versus the overall uptake m. It is shown that this novel procedure is in very good agreement with the detailed analysis of the transport parameters.

Although the studied systems are fairly different, the efficiencies of the respective methods in both cases are similar.

We have reviewed several methods that allow the determination of the transport diffusivities and surface permeabilities from transient concentration profiles. All methods exhibit similar average results with, however, significantly different accuracies as reflected by the standard deviations. In general, the accuracy of the intracrystalline concentrations as accessible by interference microscopy allows determination of the transport parameters with an uncertainty not better than 20%. The highest accuracy is attained by application of Fick's 1st law or, if the prerequisites are fulfilled, by Boltzmann's integration method. In any case, it is recommended to verify the obtained dependencies by recalculating the measured concentration profiles.

9. Conclusion

The technical application of nanoporous host materials for molecular sieving and catalysis is often determined by the transport properties of the guest molecules. The transport diffusivity as well as the surface permeability are therefore among the key properties for their practical performance. Interference microscopy has been shown to allow direct monitoring of transient, intracrystalline concentration profiles during molecular uptake and release. Thus, for the first time, the direct determination of the transport parameter has become possible.

In the present work, five different ways of determining the transport diffusivity from the concentration profiles are presented. If the prerequisites of Boltzmann's integration method are fulfilled, this method is very accurate and enables the analysis of the entire dependence of diffusivity from one single profile. The method based on Fick's 1st law is also very precise and

can be generally used without any limitations to special constraints. However, two succeeding concentration profiles (with a small time interval) are required to calculate the diffusivity. The other investigated ways of determining the diffusivity (differential application of Fick's 2nd law and the standard solution of the linear differential equation of Fick's 2nd law) show a significant scattering of the results. Also the indirect procedure, namely varying the transport parameters and searching for the best agreement between the calculated and the obtained concentration profiles, works very well. However, it requires a lot of computing time.

With the measurement of transient concentration profiles, for the first time also transport resistances on the surface of nanoporous materials may be measured directly. We present a powerful way of estimating the influence of the surface resistance on the overall uptake. It is shown that the factor by which the surface resistance retards the whole transport process can be easily deduced from a representation of the actual boundary concentration versus the overall uptake. The thus accessible information is shown to be in excellent agreement with the detailed analysis of the intracrystalline diffusivity and the surface resistance.

Acknowledgments

We thank Pavel Kortunov, Despina Tzoulaki and Christian Chmelik for many stimulating discussions. Financial support by the Studienstiftung des deutschen Volkes and by the DFG- and NWO-sponsored International Research Training Group 'Diffusion in Porous Materials' is gratefully acknowledged.

Supplement: The finite difference solution of Fick's 2nd law

The numerical solution of Fick's 2nd law (equation (S.26)) is based on Taylor expansions of the temporal and spatial dependencies of the concentration [30].

$$\frac{\partial c}{\partial t} = \frac{\partial}{\partial y}\left(D\frac{\partial c}{\partial y}\right). \tag{S.26}$$

The temporal dependency of the concentration is represented by

$$c(t+\Delta t) = c(t) + \Delta t \cdot \left(\frac{\partial c}{\partial t}\right) + \frac{\Delta t^2}{2} \cdot \left(\frac{\partial^2 c}{\partial t^2}\right) + O\left(\Delta t^3\right). \tag{S.27}$$

Neglecting the terms of second and higher order, the first temporal derivative equals

$$\frac{\partial c}{\partial t} = \frac{c(t+\Delta t) - c(t)}{\Delta t}. \tag{S.28}$$

The Taylor expansions concerning the space yield

$$u(y+\Delta y) = u(y) + \Delta y \cdot \left(\frac{\partial u}{\partial y}\right) + \frac{\Delta y^2}{2} \cdot \left(\frac{\partial^2 u}{\partial y^2}\right) + O\left(\Delta y^3\right) \tag{S.29}$$

and

$$u(y-\Delta y) = u(y) - \Delta y \cdot \left(\frac{\partial u}{\partial y}\right) + \frac{\Delta y^2}{2} \cdot \left(\frac{\partial^2 u}{\partial y^2}\right) - O\left(\Delta y^3\right). \tag{S.30}$$

Neglecting the terms of third and higher order, the difference yields

$$\left(\frac{\partial u}{\partial y}\right) = \frac{u(y+\Delta y) - u(y-\Delta y)}{2\Delta y}. \tag{S.31}$$

If we insert $u(y) = c(y)$ and $u(y) = D \cdot (\partial c/\partial y)$, equation (S.26) can be expressed as

$$\frac{c(t+\Delta t) - c(t)}{\Delta t} = \frac{\left[\begin{array}{l} D\,(c(y+\Delta y))\,(c(y+2\Delta y) - c(y))/(2\Delta y) \\ -D\,(c(y-\Delta y))\,(c(y) - c(y-2\Delta y))/(2\Delta y) \end{array}\right]}{2\cdot\Delta y}. \tag{S.32}$$

For the numerical calculation, we define a lattice for the concentration, $c_{i,j}$, with i denoting the space and j the time. By substituting Δy by $2\Delta y$, equation (S.32) can be transformed to

$$c_{i,j+1} = c_{i,j} + \frac{\Delta t}{(\Delta y)^2}\left(\frac{D\left(c_{i+1,j}\right) + D\left(c_{i,j}\right)}{2}\left(c_{i+1,j} - c_{i,j}\right) + \frac{D\left(c_{i-1,j}\right) + D\left(c_{i,j}\right)}{2}\left(c_{i-1,j} - c_{i,j}\right)\right). \tag{S.33}$$

The surface barrier, which occurs in many diffusion systems, is treated in a similar way.

Therefore, by using Fick's 1st law, the boundary condition

$$j = -\alpha(c_{\mathrm{eq}} - c_{\mathrm{surf}}) \tag{S.34}$$

can be expressed by

$$\frac{c_{i_{\max}+1} - c_{i_{\max}-1}}{2\Delta y} = \frac{\alpha}{D}\left(c_{\mathrm{eq}} - c_{i_{\max}}\right). \tag{S.35}$$

The point $i_{\max}+1$ is not a real lattice. However, the introduction of this fictive lattice point increases the accuracy.

Inserting equation (S.35) in (S.33) yields the term to calculate the boundary concentration

$$c_{i_{\max},j+1} = c_{i_{\max},j} + \frac{2\Delta t}{(\Delta y)^2}\left(\frac{D\left(c_{i_{\max}-1,j}\right) + D\left(c_{i_{\max},j}\right)}{2}\cdot\left(c_{i_{\max}-1,j} - c_{i_{\max},j}\right) + \alpha\cdot\Delta y\cdot\left(c_0 - c_{i_{\max},j}\right)\right). \tag{S.36}$$

With these equations (equations (S.33) and (S.36)), the profiles evolving during the intracrystalline mass transport can be calculated. The following algorithm shows the calculation of the profiles explicitly (the commands are valid in Mathematica 5.0).

```
tmax=2500;                                          (Set time range in seconds)
l=20*10^-6;                                         (Set half channel length in metre)
maxnx=20                                            (Set number of lattice places)
dx=l/maxnx;                                         (Calculates size of lattice steps in metre)
ce=1; c0=0;                                         (Set equilibrium and initial concentration)
diffusivity[c_]=Exp[c]*10^-13;                      (Set the transport diffusivity in
                                                    m^2 s^-1)
alpha[c_]=(1+4*c)/5*10^-7;                          (Set the surface permeability in
                                                    m s^-1)
diffmax=Max[Table[diffusivity[c],{c,c0,ce,0.01}]];
alphamax=Max[Table[alpha[c],{c,c0,ce,0.01}]];
dt=10;
While[dt*diffmax/dx^2>0.25,dt=dt/2];
While[dt*alphamax/dx>0.25,dt=dt/2];                 (Calculate size of time steps (in
                                                    seconds) to ensure convergence criteria)
For[nx=(-maxnx-1),nx<maxnx,nx=nx+1;c[nx]=c0];       (Set all initial concentrations)
maxnt=tmax/dt;
For[nt=0,nt<maxnt,nt=nt+1;                          (Start time loop)
c1[maxnx]=c[maxnx]+2*dt/(dx^2)*((c[maxnx-1]-c[maxnx])*
(diffusivity[c[maxnx]]+diffusivity[c[maxnx-1]])/2
-alpha[c[maxnx]]*dx*(c[-maxnx]-ce));                (Calculate boundary concentration)
c[-1]=c[1];                                         (Symmetry condition in the centre)
For[nx=maxnx,nx>-1,nx=nx-1;                         (Start space loop)
c1[nx]=c[nx]+dt/dx^2*((diffusivity[c[nx]]+diffusivity[c[nx+1]])/2*
(c[nx+1]-c[nx])+(diffusivity[c[nx]]+diffusivity[c[nx-1]])/2*
(c[nx-1]-c[nx]));                                   (Calculate new concentration)
];                                                  (End space loop)
For[nx=-maxnx-1,nx<maxnx,nx=nx+1;c[nx]=N[c1[Abs[nx]]]];  (Symmetry condition)
];                                                  (End time loop)
```

References

[1] Laeri F, Schüth F, Simon U and Wark M 2003 *Host–Guest Systems Based on Nanoporous Crystals* (Weinheim: Wiley-VCH)

[2] Schüth F, Sing K S W and Weitkamp J 2002 *Handbook of Porous Solids* (Weinheim: Wiley-VCH)

[3] Weitkamp J and Puppe L 1999 *Catalysis and Zeolites* (Berlin: Springer)

[4] Kärger J and Vasenkov S 2005 *Microporous Mesoporous Mater.* **85** 195

[5] Ruthven D M and Post M F M 2001 *Introduction to Zeolite Science and Practice* ed H van Bekkum, E M Flanigen, P A Jacobs and J C Jansen (Amsterdam: Elsevier)

[6] Beerdsen E, Dubbeldam D and Smit B 2006 *Phys. Rev. Lett.* **96** 044501

[7] Hahn K, Kärger J and Kukla V 1996 *Phys. Rev. Lett.* **76** 2762

[8] Saravanan C, Jousse F and Auerbach S M 1998 *Phys. Rev. Lett.* **80** 5754

[9] Kärger J, Vasenkov S and Auerbach S M 2003 *Handbook of Zeolite Science and Technology* ed S M Auerbach, K A Carrado and P K Dutta (New York: Marcel Dekker)

[10] Kärger J, Valiullin R and Vasenkov S 2005 *New J. Phys.* **7** 15

[11] Ramanan H, Auerbach S M and Tsapatsis M 2004 *J. Phys. Chem.* B **108** 17171

[12] Chen N Y, Degnan T F and Smith C M 1994 *Molecular Transport and Reaction in Zeolites* (New York: Wiley-VCH)
[13] Kärger J and Ruthven D M 1992 *Diffusion in Zeolites and Other Microporous Solids* (New York: Wiley)
[14] Jobic H and Theodorou D N 2006 *J. Phys. Chem.* B **110** 1964
[15] Schemmert U, Kärger J, Krause C, Rakoczy R A and Weitkamp J 1999 *Europhys. Lett.* **46** 204
[16] Kortunov P, Vasenkov S, Chmelik C, Kärger J, Ruthven D M and Wloch J 2004 *Chem. Mater.* **16** 3552
[17] Stapf S and Han S 2006 *NMR Imaging in Chemical Engineering* (Weinheim: Wiley-VCH)
[18] Gladden L F 2003 *AIChE J.* **49** 2
[19] Bär N K, Bauer F, Ruthven D M and Balcom B J 2002 *J. Catal.* **208** 224
[20] Schumacher R R, Anderson B G, Noordhoek N J, de Gauw F J M M, de Jong A M, de Voigt M J A and van Santen R A 2000 *Microporous Mesoporous Mater.* **6** 315
[21] Karge H G, Niessen W and Bludau H 1996 *Appl. Catal.* A **146** 339
[22] Baerlocher C, McCusker L B and Olson D H 2007 *Atlas of Zeolite Framework Types* 6th edn (Amsterdam: Elsevier)
[23] Kärger J, Kortunov P, Vasenkov S, Heinke L, Shah D B, Rakoczy R A, Traa Y and Weitkamp J 2006 *Angew. Chem. Int. Edn. Engl.* **45** 7846
[24] Kortunov P, Heinke L, Vasenkov S, Chmelik C, Shah D B, Kärger J, Rakoczy R A, Traa Y and Weitkamp J 2006 *J. Phys. Chem.* B **110** 23821
[25] Kortunov P, Heinke L, Arnold M, Nedellec Y, Jones D J, Caro J and Kärger J 2007 *J. Am. Chem. Soc.* **129** 8041
[26] Fick A 1855 *Ann. Phys. Chem.* **94** 59
[27] Kärger J 2007 *Leipzig, Einstein, Diffusion* (Leipzig: Universitätsverlag)
[28] Heinke L, Kortunov P, Tzoulaki D, Castro M J, Wright P A and Kärger J 2008 *Europhys. Lett.* **81** 26002
[29] Lehmann E, Vasenkov S, Kärger J, Zadrozna G and Kornatowski J 2003 *J. Chem. Phys.* **118** 6129
[30] Crank J 1975 *The Mathematics of Diffusion* (Oxford: Clarendon)
[31] Heinke L, Chmelik C, Kortunov P, Shah D B, Brandani S, Ruthven D M and Kärger J 2007 *Microporous Mesoporous Mater.* **104** 18
[32] Boltzmann L 1894 *Wiedemanns Ann. Phys.* **53** 959
[33] Jost W 1960 *Diffusion in Solids, Liquids and Gases* (New York: Academic)
[34] Kortunov P, Heinke L and Kärger J 2007 *Chem. Mater.* **19** 3917
[35] Heinke L 2007 *Diffus. Fundam.* **4** 9.1
[36] Bronstein I N, Semendjajew K A, Musiol G and Mühlig H 2001 *Taschenbuch der Mathematik* 5th edn (Frankfurt: Harri Deutsch)
[37] Stenlund H 2005 *Three Methods for Solutions of Concentration Dependent Diffusion Coefficient* Visilab Signal Technologies, Finland http://www.visilab.fi/bolmatano.pdf
[38] Tzoulaki D, Heinke L, Schmidt W, Wilczok U and Kärger J 2008 *Angew. Chem. Int. Edn. Engl.* at press
[39] Heinke L, Kortunov P, Tzoulaki D and Kärger J 2007 *Adsorption* **13** 215–23
[40] Heinke L 2007 *Diffus. Fundam.* **4** 12.1
[41] Heinke L, Kortunov P, Tzoulaki D and Kärger J 2007 *Phys. Rev. Lett.* **99** 228301